


Phase diagram of the dynamics of a precessing qubit under a quantum measurementXinru Tang and Fuxiang Li ^{*}*School of Physics and Electronics, Hunan University, Changsha 410082, China*

(Received 19 March 2020; accepted 14 May 2020; published 1 June 2020)

We study the phase transitions induced by sequentially measuring a single qubit precessing under an external transverse magnetic field. Under projective quantum measurement, the probability distribution of the measurement outcomes can be mapped exactly to the thermodynamic probability distribution of a one-dimensional Ising model, whose coupling can be varied by the magnetic field from ferromagnetic to antiferromagnetic. For the general case of sequential quantum measurement, we develop a fast and exact algorithm to calculate the probability distribution function of the ferromagnetic order and antiferromagnetic order, and a phase diagram is obtained in the parameter space spanned by the measurement strength and magnetic field strength. The mapping to a long-range interacting Ising model is obtained in the limit of small measurement strength. Full counting statistical approach is applied to understand the phase diagram and to make connections with the topological phase transition that is characterized by the braid group. This work deepens our understanding of phase transitions induced by quantum measurement and may provide another method to characterize and steer the quantum evolution.

DOI: [10.1103/PhysRevA.101.062102](https://doi.org/10.1103/PhysRevA.101.062102)**I. INTRODUCTION**

Quantum measurement is one of the most intriguing properties in quantum mechanics [1–4]. The understanding and utilization of quantum measurement is crucial to the future application of quantum information and quantum computation [5], quantum cryptography [6], and quantum sensing [7]. Quantum measurements can be either strong or weak, depending on the specific system and purpose of application. For strong measurement, it is usually applied in initializing and reading out quantum states [8–14]. For weak quantum measurement, it is particularly useful for monitoring quantum evolution [15–19], maneuvering quantum state [20–22], and studying the entanglement and correlation propagation in quantum many-body systems [23–25]. More recently, great efforts have been devoted to the development of different experimental techniques to detect the single-qubit dynamics [26–32] and to characterize the decoherence induced by environments [33–35]. In the context of quantum measurement, the idea of dynamical phase transition and thermodynamics of quantum jump trajectories was also proposed [36]. Backaction of measurement on the many-body system induces nontrivial dynamical effects such as long-range entanglement and correlated tunneling [37]. Moreover, interplay between measurement and the intrinsic interaction yields different kinds of phase transitions [38] and exotic universality class of critical phenomena in non-Hermitian systems [39].

Continuous or sequential quantum measurement has been theoretically studied using different approaches, like random walks in state space [40], quantum Bayesian approach [41], and stochastic path-integral formalism [42,43]. Recently, it was theoretically discovered that the language of phase

transition can be used to distinguish the weak and strong measurements by mapping the probability distribution of sequential measurement outputs to the thermodynamic distribution of interacting Ising spin models [44]. The authors find that, for a single qubit or a two-level system under sequential quantum measurement, the boundary between weak and strong measurements can be very well defined by a critical value of measurement strength or duration. However, their study is mainly focused on a qubit without any dynamics. One would expect that there exist richer and more interesting phase transition behaviors if the qubit experiences its own dynamics besides that induced by measurement. Indeed, it was theoretically discovered that, in the presence of an external transverse magnetic field, the qubit dynamics may undergo a phase transition between coherent oscillation and quantum Zeno effect, induced by sequential weak measurement [45]. Furthermore, it was later found that this phase transition is associated with a topological transition that can be classified by different elements of the braid group [46].

In this paper, we study the interplay of external magnetic field and sequential quantum measurement on the dynamics of a single qubit, by mapping the measurement outcomes to the on-site spin states of a one-dimensional (1D) Ising spin model. We find that the presence of a transverse magnetic field introduces an additional degree of freedom that induces the phase transition among the ferromagnetic, paramagnetic, and antiferromagnetic phases. We develop a fast and exact algorithm to calculate the probability distribution of the ferromagnetic order and antiferromagnetic order and thus to determine the phase diagram in the parameter space spanned by field strength and measurement strength. In the limit of small measurement strength, the probability distribution can be mapped to a long-range Ising spin model, which can help us understand the phase diagram. Moreover, using the full counting statistical approach, we can analytically obtain

^{*}fuxiangli@hnu.edu.cn

the probability distribution in the limiting cases of small measurement strength and field strength, which helps us make a connection with the topological phase transition discovered in Ref. [46]. Our findings provide deeper understanding in the phase transitions induced by quantum measurements.

The paper is organized as follows. In Sec. II, we present the formalism that is needed to describe the dynamics of a single qubit under quantum measurement and external transverse magnetic field. In Sec. III, we discuss the phase transition when the qubit is monitored by projective measurement. In Sec. IV, we develop the fast algorithm to calculate the probability distributions of ferromagnetic order and antiferromagnetic order and obtain the phase diagram. We further find a long-range interacting Ising model than can capture physics in the case of small measurement strength. Furthermore, a full counting statistical approach is applied to obtain analytical expressions of probability distribution in the limiting case of small measurement strength and field strength. In Sec. V, the cases with different initial states and with nonzero relaxation rates are discussed. Conclusions are made in the last section.

II. FORMALISM OF MEASURING A PRECESSING SINGLE QUBIT

We consider the dynamics of a single qubit under a transverse magnetic field in the \hat{y} direction. Its Hamiltonian is expressed as

$$\hat{H} = \frac{1}{2}\hbar\omega_L\hat{\sigma}_y, \quad (1)$$

in which $\hat{\sigma}_y$ is the y -component Pauli matrices and ω_L is the Larmor frequency. Without quantum measurement, the density matrix $\hat{\rho}$ that describes the quantum state of the qubit undergoes a unitary evolution, and it can be formally written as

$$\hat{\rho}(t) = e^{-i\hat{H}t}\hat{\rho}_0e^{i\hat{H}t}, \quad (2)$$

with $\hat{\rho}_0$ being the initial density matrix and $\hat{U}(t) = e^{-i\hat{H}t}$ being the unitary evolution operator. In terms of Pauli matrices, the single-qubit density matrix can always be represented by four real parameters, ρ_0 and $\boldsymbol{\rho} \equiv \{\rho_x, \rho_y, \rho_z\}$:

$$\hat{\rho} = \frac{1}{2}[\rho_0\hat{1} + \boldsymbol{\rho} \cdot \hat{\boldsymbol{\sigma}}]. \quad (3)$$

Starting from initial-state vector $\{\rho_0, \rho_x, \rho_y, \rho_z\}$, the density matrix becomes, after revolution time τ ,

$$\begin{aligned} \hat{\rho}(\tau) = & \rho_0\hat{1} + [\rho_x \cos(\omega) + \rho_z \sin(\omega)]\hat{\sigma}_x \\ & + [\rho_z \cos(\omega) - \rho_x \sin(\omega)]\hat{\sigma}_z + \rho_y\hat{\sigma}_y. \end{aligned} \quad (4)$$

Here we introduce a parameter ω to describe the strength of external magnetic field:

$$\omega = \omega_L\tau. \quad (5)$$

Together with the measurement strength, it will induce the phase transitions among ferromagnetic, paramagnetic, and antiferromagnetic phases. Note that since the qubit precesses around the transverse magnetic field in the y direction, the y component of the density matrix would not change, and thus can be set to be zero, $\rho_y(t) = 0$.

We adopt a sequential measurement scheme, described by a series of commuting POVM operators [15,40],

$$\hat{M}_\alpha = \frac{1}{\sqrt{2}}\left(\sin\frac{\theta}{2}\hat{1} + \alpha\cos\frac{\theta}{2}\hat{\sigma}_z\right), \quad (6)$$

with $\alpha = \pm 1$ being the measurement outcomes. This measurement scheme allows us to consider both the weak and strong measurements with adjustable measurement strength $\lambda = \sin\theta$ ranging from 0 to 1 when θ ranges from 0 to $\pi/2$. Under a single quantum measurement, the probability of obtaining outcome α is given by

$$P_\alpha = \text{Tr}[\hat{M}_\alpha\hat{\rho}\hat{M}_\alpha^\dagger], \quad (7)$$

and the normalized density operator after measurement becomes

$$\hat{\rho}' = \hat{M}_\alpha\hat{\rho}\hat{M}_\alpha^\dagger/P_\alpha. \quad (8)$$

After a series of such measurements with equal time interval τ and unitary evolution under transverse magnetic field ω_L in between, the combined evolution of density matrix can be formally expressed as

$$\hat{\rho} = \hat{M}_{\alpha_N}\hat{U}_N\dots\hat{M}_{\alpha_1}\hat{U}_1\hat{\rho}_0\hat{U}_1^\dagger\hat{M}_{\alpha_1}^\dagger\dots\hat{U}_N^\dagger\hat{M}_{\alpha_N}^\dagger/P_\alpha. \quad (9)$$

Here, N is the total number of measurements, and P_α is the probability of obtaining a specific series of outcomes $\boldsymbol{\alpha} = \{\alpha_1, \alpha_2, \dots, \alpha_N\}$, given by

$$P_\alpha = \text{Tr}[\hat{M}_{\alpha_N}\hat{U}_N\dots\hat{M}_{\alpha_1}\hat{U}_1\hat{\rho}_0\hat{U}_1^\dagger\hat{M}_{\alpha_1}^\dagger\dots\hat{U}_N^\dagger\hat{M}_{\alpha_N}^\dagger]. \quad (10)$$

Since the y component of density matrix can be set to be zero, we introduce a three-component vector to describe the state of the qubit: $\mathbf{p} \equiv \{\rho_0, \rho_z, \rho_x\}$. Starting immediately after the $(n-1)$ -th measurement with vector \mathbf{p}_{n-1} , the state experiences a precession ω of time τ and then is followed by the n th measurement \hat{M}_{α_n} . The new vector \mathbf{p}_n evolves in the following way:

$$\mathbf{p}_n = \mathcal{A}_{\alpha_n}\mathbf{p}_{n-1} \quad (11)$$

with the ‘‘evolving matrix’’

$$\mathcal{A}_\alpha = \frac{1}{2}\begin{pmatrix} 1 & \alpha\sin\theta\cos\omega & -\alpha\sin\theta\sin\omega \\ \alpha\sin\theta & \cos\omega & -\sin\omega \\ 0 & \cos\theta\sin\omega & \cos\theta\cos\omega \end{pmatrix}. \quad (12)$$

It contains α as the outcome, and two parameters θ and ω describing the measurement strength and the strength of transverse field, respectively. It should be emphasized that Eq. (12) describes the conditioned evolution of qubit state vector \mathbf{p}_n . The conservation of total probability is guaranteed by noting that, after the n th measurement, the total probability is the sum of the two probabilities with outcomes $\alpha = \pm 1$. Thus, $P_n = (\mathcal{A}_+\mathbf{p}_{n-1})_{11} + (\mathcal{A}_-\mathbf{p}_{n-1})_{11} = (\mathbf{p}_{n-1})_{11} \equiv P_{n-1}$.

In this paper, we will utilize this evolving matrix to analyze the probability distribution of the outcomes and to determine the phase transitions. However, before we discuss the general cases, we would like to, in next section, first discuss the special case of projective quantum measurement, in which the probability distribution can be easily obtained and the mapping to Ising spin model is exact.

III. PHASE TRANSITION INDUCED BY LARMOR PRECESSION AND PROJECTIVE MEASUREMENT

For projective measurement with $\theta = \pi/2$, the measurement operator reduces to

$$\hat{M}_\alpha = \frac{1}{2}[\hat{1} + \alpha\hat{\sigma}_z], \quad (13)$$

Its effect on any initial wave function is to collapse the wave function to become the eigenstate $|\alpha\rangle$ of Pauli matrix $\hat{\sigma}_z$, depending on the outcome $\alpha = \pm 1$. In the language of density matrix, the projective measurement operator \hat{M}_α reduces the state $\hat{\rho} = (1/2)(\rho_0\hat{1} + \boldsymbol{\rho} \cdot \hat{\boldsymbol{\sigma}})$ to be $\hat{\rho} = (1/2)(\hat{1} + \alpha\hat{\sigma}_z)$, with probability of obtaining outcome α , $P_\alpha = (1/2)(\rho_0 + \alpha\rho_z)$. Taking into account of the unitary evolution due to Larmor precession, one obtains the probability $P_{\alpha_0, \alpha}$ after one measurement with outcome α together with the previous outcome being α_0 :

$$P_{\alpha_0, \alpha} = \frac{1}{2}[1 + \cos(\omega)\alpha\alpha_0]. \quad (14)$$

Therefore, the probability of obtaining a series of specific outcome $\boldsymbol{\alpha}$ would be

$$P_\alpha = \frac{1}{2^N} \prod_{k=1}^N [1 + \cos(\omega)\alpha_k\alpha_{k-1}]. \quad (15)$$

This probability can be mapped exactly to the thermodynamic probability of a nearest-neighbor coupled Ising spin model described by Hamiltonian

$$H = -J \sum_{k=1}^N \alpha_k \alpha_{k-1}. \quad (16)$$

The model is defined on a 1D lattice of N sites, with each site assigned with an Ising spin $\alpha_k = \pm 1$. The probability of finding a specific spin configuration is given by the Gibbs distribution [47],

$$P_{\text{Ising}} = \frac{1}{\mathcal{Z}} e^{-\beta H} = \frac{1}{\mathcal{Z}} e^{\beta J \alpha_k \alpha_{k-1}}. \quad (17)$$

Here, β is the inverse of temperature $\beta = 1/(k_B T)$. The partition function $\mathcal{Z} = \text{Tr} e^{-\beta H}$ with the trace running over all the 2^N possible spin configurations. Setting $P_\alpha = P_{\text{Ising}}$, we arrive at the following relation:

$$\tanh(\beta J) = \cos(\omega). \quad (18)$$

This identity builds up the relation between the Larmor frequency of single qubit and the effective coupling of a 1D Ising model. When $\omega = 0$, $\beta J = \infty$, corresponding to a ferromagnetically coupled Ising spin chain with infinite coupling strength J , or with finite coupling strength J but under zero temperature. In this case, the ferromagnetic phase is very well defined. As one increases ω , the quantity βJ becomes finite, which can be understood as the increase of temperature being nonzero, thus leading to the transition into a paramagnetic phase. As ω becomes π , $\beta J = -\infty$, corresponding to antiferromagnetic coupling in the Ising model with infinite coupling strength, or finite strength but at zero temperature. In this case, the system is in the antiferromagnetic phase.

Note that a similar discussion of phase transition among the ferromagnetic, paramagnetic, and antiferromagnetic phases is made in Ref. [44]. However, this transition is induced by

the angle between sequential measurements. This needs to change the measurement axis at each time of measurement, which requires experimental technique with sufficiently high standards and precision. Otherwise, if, at each time of measurement, the angle with the previous measurement axis is not a constant, then it actually corresponds to introducing disorder in the coupling strength of the Ising model. From statistical mechanics, any amount of disorder would break the long-range ferromagnetic order in the 1D Ising model, making the phase transition difficult to observe. In our case, however, the phase transition is induced by the external magnetic field, which can be controlled in the experiment with high precision.

IV. SEQUENTIAL MEASUREMENT AND PHASE DIAGRAM

For the general cases of measurement strength θ and Larmor precession ω , the analytical approach becomes awkward and even impossible. In this section, we develop a fast algorithm which enables us to numerically and accurately determine the phase transitions. As is well known, to describe the magnetic phase transition, one needs to define a ferromagnetic order parameter M_F and antiferromagnetic order parameter M_{AF} , and study their probability distribution, which would tell us about the information of phase transition, as was revealed in Landau's theory of phase transition. Using this algorithm, we determine the phase diagram in the parameter space spanned by θ and ω . We show that this phase diagram can be quantitatively understood from the long-range Ising spin model and from the full counting statistical approach.

A. Recursion relation

Specifically for the definition of ferromagnetic order, we assume N measurements, or N sites in the language of Ising model. Then we can define the ferromagnetic order as $M_F = (N_\uparrow - N_\downarrow)/N$, with $N_{\uparrow, \downarrow}$ being the number of sites with spin up (down), or the number of outcomes $\alpha = \pm 1$, respectively. We define a probability $P(n_\uparrow, n)$ denoting the probability of obtaining n_\uparrow outcomes of $\alpha = +1$ after n measurements. It is actually nothing but the first component of state vector $\mathbf{P}(n_\uparrow, n) \equiv \{\rho_0, \rho_z, \rho_x\}$, which describes the conditioned state vector after n measurements and with n_\uparrow outcomes of $\alpha = +1$. Given the evolving matrix \mathcal{A}_α in Eq. (12), the conditioned state vector $\mathbf{P}(n_\uparrow, n)$ is given by the following recursion relation:

$$\mathbf{P}(n_\uparrow, n+1) = \mathcal{A}_+ \mathbf{P}(n_\uparrow - 1, n) + \mathcal{A}_- \mathbf{P}(n_\uparrow, n). \quad (19)$$

The initial condition is simply $\mathbf{P}(n_\uparrow, n=0) = \delta_{n_\uparrow, 0} \mathbf{p}_0$ with $\mathbf{p}_0 = \{\rho_0(0), \rho_z(0), \rho_x(0)\}$ being the initial state vector. This recursion relation can be understood in the following way. Immediately after $(n+1)$ -th measurement, the probability of obtaining n_\uparrow number of up spins has two contributions: one is from the previous probability $\mathbf{P}(n_\uparrow - 1, n)$ of obtaining $n_\uparrow - 1$ up spins together with the $(n+1)$ -th measurement to be up (given by \mathcal{A}_+), the other is from the previous probability $\mathbf{P}(n_\uparrow, n)$ of obtaining n_\uparrow up spins together with the $(n+1)$ -th outcome to be down (given by \mathcal{A}_-).

After N measurements, we come to a probability vector $\mathbf{P}(N_\uparrow, N)$ describing the probability with N_\uparrow outcomes of

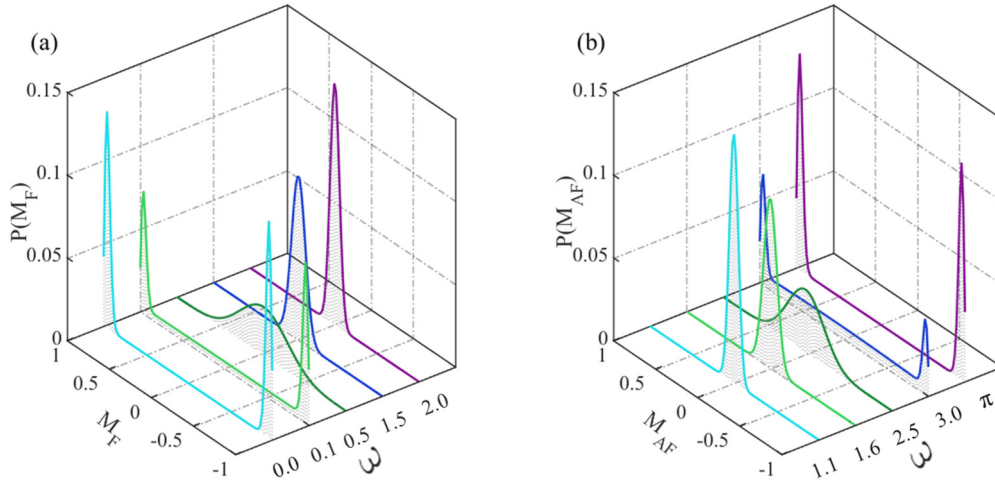


FIG. 1. Phase transitions revealed by the probability distribution of ferromagnetic order M_F (a) and antiferromagnetic order M_{AF} (b). Panel (a) shows the transition from the polarized (PL) phase with two peaks at $M_F \neq 0$, to the unpolarized (UPL) phase with only one peak centered exactly at $M_F = 0$, as one increases the value of ω . From left to right, we fix $\theta = 2\pi/5$, and vary ω to be 0.0, 0.1, 0.5, 1.5, 2.0. Panel (b) shows the transition from the unpolarized phase with one peak centered at $M_{AF} = 0$, to the antipolarized (APL) phase with two peaks at $M_{AF} \neq 0$. Again, we fix $\theta = 2\pi/5$, and vary ω to be 1.1, 1.6, 2.5, 3.0, π from left to right. Note that all the variables, such as ω , M_F , M_{AF} , and $P(M_F)$, are unitless.

$\alpha = +1$. The first component is just $P(n_\uparrow, n)$ that we are desired for, from which a symmetry-breaking phenomena can be observed, as is illustrated in Fig. 1(a), in which we plot this probability distribution as function of $M_F = (N_\uparrow - N_\downarrow)/N$ for different values of ω and θ . Clearly a transition from two peaks to one peak is observed, as we fix the value of θ but increase ω . The position of maximal probability transits from $N_\uparrow^{(\max)} \neq N/2$ to exactly $N_\uparrow^{(\max)} = N/2$, corresponding to the transition from nonzero ferromagnetic order $M_F \neq 0$ to exactly $M_F = 0$.

For the definition of antiferromagnetic order parameter, we divide the N sites into $N/2$ unit cells, with each unit cell consisting of two nearest neighbor sites. There are in total four cases of spin configurations $\{\uparrow\uparrow\}$, $\{\uparrow\downarrow\}$, $\{\downarrow\uparrow\}$, and $\{\downarrow\downarrow\}$ in one unit cell. Then we define the AFM order to be $M_{AF} = (N_{\uparrow\downarrow} - N_{\downarrow\uparrow})/(N/2)$, with $N_{\uparrow\downarrow}$ ($N_{\downarrow\uparrow}$) being the number of unit cells with the two neighboring spins in state $\{\uparrow\downarrow\}$ ($\{\downarrow\uparrow\}$).

Using similar procedure to the case of ferromagnetic order, we develop an algorithm to calculate the probability distribution of antiferromagnetic order M_{AF} . For this purpose, we first define a quantity $n_A = n_{\uparrow\downarrow} - n_{\downarrow\uparrow}$, with $n_{\uparrow\downarrow}$ ($n_{\downarrow\uparrow}$) being the number of unit cells with the two neighboring spins in state $\{\uparrow\downarrow\}$ ($\{\downarrow\uparrow\}$). Then we study the probability distribution $P_A(n_A, n)$, meaning the probability of obtaining n_A after $2n$ measurements. The recursion relation for the corresponding conditioned state vector $\mathbf{P}(n_A, n)$ can be readily written as

$$\mathbf{P}_A(n_A, n+1) = \mathcal{A}_P \mathbf{P}_A(n_A, n) + \mathcal{A}_+ \mathcal{A}_- \mathbf{P}_A(n_A - 1, n) + \mathcal{A}_- \mathcal{A}_+ \mathbf{P}_A(n_A + 1, n), \quad (20)$$

with the parallel measurement operator given by

$$\mathcal{A}_P = \mathcal{A}_+^2 + \mathcal{A}_-^2. \quad (21)$$

It means that at $(n+1)$ -th unit cell, or at $2(n+1)$ -th measurements, the conditioned state vector $\mathbf{P}_A(n_A, n+1)$ of obtaining n_A is contributed from three sources: The first is from

$\mathbf{P}_A(n_A, n)$ with same number of n_A together with the outcome of the n th unit cell being in state $\{\uparrow\uparrow\}$ or in state $\{\downarrow\downarrow\}$, the second is from the probability $\mathbf{P}_A(n_A - 1, n)$ together with the outcome of n th unit cell being in state $\{\uparrow\downarrow\}$ (contributing $\mathcal{A}_+ \mathcal{A}_-$), and the last is from the probability $\mathbf{P}_A(n_A + 1, n)$ together with the outcome of n th unit cell being in state $\{\downarrow\uparrow\}$ (contributing $\mathcal{A}_- \mathcal{A}_+$).

After N measurements, we obtain the probability $P_A(N_A, N/2)$ which is just the probability distribution $P_A(M_{AF}, N)$ of the antiferromagnetic order $M_{AF} = N_A/(N/2)$. We plot this probability distribution for different values of ω but with fixed θ in Fig. 1(b), and observe that there is indeed a transition from two peaks located at $M_{AF} \neq 0$ to one peak centered at $M_{AF} = 0$.

B. Phase diagram

In order to quantitatively characterize these two transitions in terms of the probability distribution, we define three phases, polarized (PL) phase, unpolarized (UPL) phase, and antipolarized (APL) phase, and obtain the phase diagram in the θ - ω plane. From the probability distribution $P(M_F, N)$ of ferromagnetic order M_F , we can define the PL phase if the maximal probability is located at nonzero value $M_F \neq 0$. From the probability distribution of $P_A(M_{AF}, N)$ of the antiferromagnetic order M_{AF} , we can define the APL phase if the maximal probability is located at nonzero value of $M_{AF} \neq 0$. Otherwise, if both the maximum of $P(M_F, N)$ is located at $M_F = 0$ and that of $P_A(M_{AF}, N)$ at $M_{AF} = 0$, then we call UPL phase.

In Fig. 2, based on the calculations using the fast algorithm, we present the phase diagram for two different values of $N = 100$ [Fig. 2(a)] and $N = 1000$ [Fig. 2(b)]. It is clear that, for a fixed measurement strength θ , as one increases the Larmor precession ω , the system undergoes in sequence the three phases, PL, UPL, and APL. There are two points worth

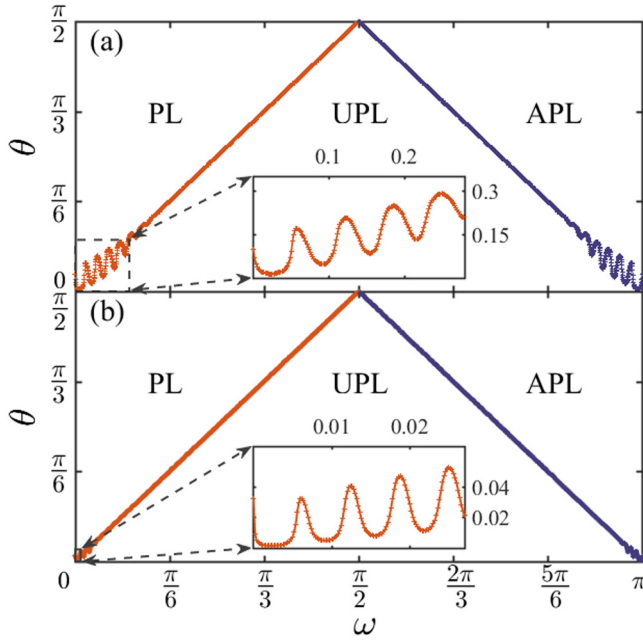


FIG. 2. Phase diagram in the θ - ω plane, for two cases of $N = 100$ (a) and $N = 1000$ (b). The insets are enlargements of the oscillations that appear in the region of small θ and ω . Initial state is $\mathbf{p}_0 = \{1, 0, 1\}$, and relaxation rate is zero.

noting. First, for small N , the finite-size effect is obvious. Especially for the region of small θ and ω , there appears an oscillation with a certain oscillation period. As shown in Fig. 2, the period of oscillation is about 0.063 for $N = 100$ [see the inset in Fig. 2(a)] and 0.0063 for $N = 1000$ [see the inset in Fig. 2(b)]. As will be discussed in next subsection, this oscillation behavior can be understood from a long-range interacting Ising model, and the period is found to be roughly $2\pi/(N-2)$, which agrees well with our numerical results. Second, for large N , the finite-size effect becomes diminished, and the phase boundary is almost a straight line, defined by $\omega = \theta$ for the PL/UPL phase boundary, and $\theta = \pi - \omega$ for the UPL/APL phase boundary. The boundary can be understood from analytical analysis by using the full counting statistical approach.

C. Long-range interacting Ising model

The phase diagram obtained by numerical calculation can be quantitatively understood by deriving a long-range interacting Ising model in the limit of weak measurement strength $\theta \ll 1$. From Eq. (12), one can obtain the final-state vector \mathbf{p}_N after N measurements with a specific series of outcomes $\boldsymbol{\alpha}$ in a form like

$$\mathbf{p}_N(\boldsymbol{\alpha}) = \mathcal{A}_{\alpha_N} \dots \mathcal{A}_{\alpha_2} \mathcal{A}_{\alpha_1} \mathbf{p}_0. \quad (22)$$

In general, the mathematical form is too complicated to give rise to a compact analytical result. However, in the limit of $\theta \ll 1$, one is lucky to find that the probability is given by

$$P(\boldsymbol{\alpha}) \sim e^{\theta^2 \sum_{j < k} \cos[(k-j-1)\omega] \alpha_j \alpha_k}. \quad (23)$$

This probability distribution can be recognized as the Gibbs distribution of a long-range interacting Ising model with

Hamiltonian:

$$H = -\theta^2 \sum_{j < k}^N \cos[(k-j-1)\omega] \alpha_j \alpha_k. \quad (24)$$

For the case of $\omega = 0$, this model reduces to the long-range ferromagnetic Ising Hamiltonian obtained in Ref. [44]. More interesting cases occur with increasing ω when the long-range couplings gradually change from ferromagnetic to antiferromagnetic. The longest-range coupling is between the site 1 and N with coupling strength $J_{1,N} = \theta^2 \cos[(N-2)\omega]$. As ω increases, this coupling strength $J_{1,N}$ starts to oscillate, first decreasing from positive to negative and then increasing back to positive. The oscillation period is given by $\delta_\omega = 2\pi/(N-2)$. The other shorter range couplings also oscillate with ω , but with a smaller period. Totally, this picture gives rise to an oscillating behavior on the phase boundary. However, at larger ω , the coupling strengths of different range oscillating with different periods interfere with each other and the amplitude of oscillation in the phase boundary finally diminish, as is revealed in the phase diagram in Fig. 2.

D. Full counting statistical approach

In this subsection, we would like to understand the phase diagram by using the full counting statistical approach, in order to obtain analytical expressions for the probability distribution functions. Define the generating function for the conditioned state vector $\mathbf{P}(n_\uparrow, n)$ at the n th measurement [48],

$$\mathbf{Z}(\chi, n) = \sum_{n_\uparrow=0}^{\infty} \mathbf{P}(n_\uparrow, n) e^{i\chi n_\uparrow}. \quad (25)$$

The recursion relation (19) becomes

$$\mathbf{Z}(\chi, n) = (\mathcal{A}_+ e^{i\chi} + \mathcal{A}_-) \mathbf{Z}(\chi, n-1). \quad (26)$$

Through this method, the generating function $\mathbf{Z}(\chi, N)$ after N measurements would be readily written down. Thus, the probability $P(N_\uparrow, N)$ of obtaining N_\uparrow after N measurements would be analytically calculated from the generating function:

$$P(N_\uparrow, N) = \frac{1}{2\pi} \int_0^{2\pi} d\chi e^{-i\chi N_\uparrow} Z_0(\chi, N). \quad (27)$$

In general cases, the analytical expression for $Z_0(\chi, N)$ is difficult to obtain. However, for the limiting case with small ω and small θ , one can obtain a closed form. Indeed, in this limit, the ‘‘Hamiltonian’’ $\hat{K} = \mathcal{A}_+ e^{i\chi} + \mathcal{A}_-$ governing the dynamics of $\mathbf{Z}(\chi, n)$ reduces to

$$\hat{K}(z) = \frac{1}{2} \begin{pmatrix} z+1 & (z-1)\theta & 0 \\ (z-1)\theta & z+1 & -(z+1)\omega \\ 0 & (z+1)\omega & z+1 \end{pmatrix} \quad (28)$$

with $z = e^{i\chi}$. This ‘‘Hamiltonian’’ has three eigenvalues:

$$E_{1,2} = \frac{1}{2}[(z+1) \pm \varepsilon(z)], \quad E_3 = \frac{1}{2}(z+1), \quad (29)$$

with

$$\varepsilon(z) = \sqrt{(z-1)^2 \theta^2 - (z+1)^2 \omega^2}. \quad (30)$$

It is interesting to note that, for the first two eigenvalues, if we set $z = 0$, they reduce to $E_{1,2} = \frac{1}{2}(1 \pm \sqrt{\theta^2 - \omega^2})$,

which are real for $\theta > \omega$, but become imaginary for $\theta < \omega$, leading to quite distinguished behaviors of $\mathbf{Z}(\chi, t)$ in the large- N limit, and thus that of probability distribution function $P(N_\uparrow, N)$. Generally, the generating function $Z_0(\chi, N)$ can be written as $Z_0(\chi, N) = \sum_{j=1,2,3} c_j(\chi) E_j^N$, with c_j being the coefficients that are dependent on the initial states.

From a similar equation, we note that in Ref. [46], the authors discovered a transition from the regime with quantum mechanical coherent oscillations to the regime with a frozen dynamics, i.e., quantum Zeno effect, and it was connected to an interesting topological phase transition, described by a braiding group in the space of complex eigenvalues as functions of χ ranging from 0 and 2π . Here, our findings of the ferromagnetic-paramagnetic phase transition is closely connected to this transition, and the study of PL and UPL phases may provide another point of view for this transition, whose transition line is also defined by $\omega = \theta$.

Indeed, for simplicity, we consider the case with initial state $\hat{\rho}_0 = \frac{1}{2}(\hat{1} + \hat{\sigma}_x)$, corresponding to initial condition for $\mathbf{Z}(\chi, n = 0) = (1, 0, 1)$. The evolution can be obtained explicitly:

$$Z_0(z, N) = f_z E_3^N + \frac{1}{2}(1 - f_z)(E_1^N + E_2^N), \quad (31)$$

with

$$f_z = \frac{(z + 1)\omega}{(z - 1)\theta + (z + 1)\omega}. \quad (32)$$

In obtaining the probability distribution from Eq. (27), one can make a variable change: $z = e^{i\chi}$, thus transforming the integration to be a contour integration on the unit circle \mathcal{C} in the complex plane:

$$P(N_\uparrow, N) = \frac{1}{2\pi i} \oint_{\mathcal{C}} dz \frac{1}{z^{N_\uparrow+1}} Z_0(z, N). \quad (33)$$

In the large- N limit, we can use the stationary phase approximation to obtain analytical results. We discuss the two limiting cases with $\theta \gg \omega$ and $\theta \ll \omega$.

For the case with $\theta \ll \omega$, $f_z \rightarrow 1$, the second term in Eq. (31) vanishes compared to the first term. Then we have

$$P(N_\uparrow, N) = \frac{1}{2\pi i} \oint_{\mathcal{C}} dz \frac{1}{z^{N_\uparrow+1}} E_3^N = \frac{1}{2^{N_\uparrow}} C_N^{N_\uparrow}. \quad (34)$$

The probability distribution reduces to a binomial distribution function with only one peak located at $N_\uparrow^{(\max)} = N/2$. Therefore, this distribution function corresponds to the unpolarized phase.

For the case with $\theta \gg \omega$, $f_z \rightarrow 0$, and thus the second term proportional to $(1 - f_z)$ in Eq. (31) dominates. Near $z \sim 0$, we can approximate $\varepsilon(z)$ up to first order of z : $\varepsilon = q_2 + q_1 z$, with $q_1 = \frac{\theta^2 + \omega^2}{\sqrt{\theta^2 - \omega^2}}$ and $q_2 = \sqrt{\theta^2 - \omega^2}$. Then we obtain

$$P(N_\uparrow, N) = \frac{1}{2^{N_\uparrow+1}} C_N^{N_\uparrow} [(1 + q_1)^{N_\uparrow} (1 - q_2)^{N - N_\uparrow} + (1 - q_1)^{N_\uparrow} (1 + q_2)^{N - N_\uparrow}]. \quad (35)$$

In this case, the distribution function is a combination of two binomial distribution functions. In the large- N limit, it corresponds to two peaks located at

$$N_\uparrow^{(\max)} = \frac{1 + q_1}{2 + q_1 - q_2} N, \text{ and } \frac{1 - q_1}{2 - q_1 + q_2} N, \quad (36)$$

which are no longer $N/2$.

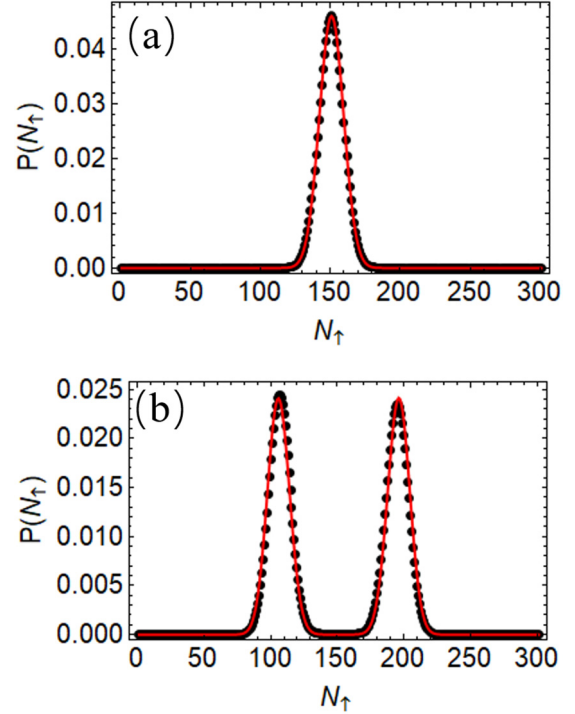


FIG. 3. The probability distribution obtained from the analytical results (red lines) are compared with the exact numerical calculations (black dots). Distribution function (34) is used in panel (a) with parameters $\theta = 0.01$ and $\omega = 0.2$, while Eq. (35) is used in panel (b) with $\theta = 0.3$ and $\omega = 0.001$.

The above two results are plotted in Fig. 3 together with that obtained from exact numerical calculations. It is seen that the analytical result agrees well with numerical results.

V. DISCUSSIONS

It is worth noting that in Ref. [36], the authors applied the large deviation (LD) method to study the dynamics of quantum trajectory ensembles and observed a similarity between the dynamical order parameters and the order parameters that are considered in equilibrium statistical properties of ensembles of configurations. The procedure they adopted is similar to the full counting statistics we used in the present paper. However, the findings are quite different. In Ref. [36], the formal similarity is observed between the LD function of trajectories and free energy of equilibrium statistical mechanics, and then a dynamical phase transition or phase crossover is identified. Moreover, this phase transition is well defined only for a quantum system with more than two degrees of freedom. That is, it does not exist in the two-level system under continuous observation, the system that is our study object in the present paper. In our case, the mapping of the measurement outcomes to 1D Ising spin model is direct and well established, and a long-range coupled Ising spin Hamiltonian is presented. Given this, the correlation between each measurement outcome can be studied, and the phase transition is also defined, just in the same way as that in equilibrium statistical mechanics.

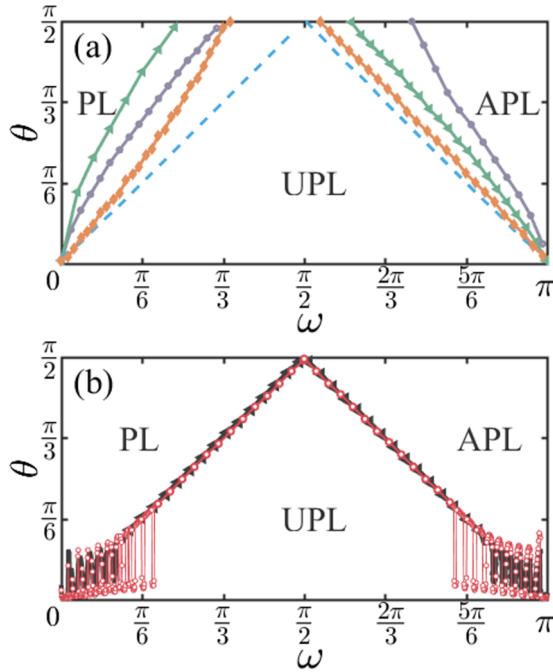


FIG. 4. The phase diagram with different initial states (a) and different relaxation rates (b). For panel (a), the initial states are, respectively, $\mathbf{p}_0 = (1, 1/2, \sqrt{3}/2)$ (the orange line with diamonds), $\mathbf{p}_0 = (1, \sqrt{3}/2, 1/2)$ (the gray line with circles), and $\mathbf{p}_0 = (1, 1, 0)$ (the green line with triangles), together with $\mathbf{p}_0 = (1, 0, 1)$ (the dashed blue line). Here, the number of measurements is $N = 1000$. For panel (b), the initial states are $\mathbf{p}_0 = (1, 1, 0)$, and $N = 100$, with different relaxation rates $r = 0.01$ (the black line with triangles) and $r = 0.02$ (the red line with hollow circles).

Until now, our studies are mainly focused on the situation with initial state $\hat{\rho}_0 = \frac{1}{2}(\hat{1} + \hat{\sigma}_x)$ and with relaxation rate set to be zero. To complete our studies, we would like to briefly discuss the effects of different initial quantum states and additional relaxation rate on the phase diagram.

First, we plot the phase diagram for different initial states in Fig. 4(a). Besides the state $\mathbf{p}_0 = (1, 0, 1)$ denoting the initial spin pointing to x direction, we choose three other initial states to be $\mathbf{p}_0 = (1, 1/2, \sqrt{3}/2)$ (red), $\mathbf{p}_0 = (1, \sqrt{3}/2, 1/2)$ (gray), and $\mathbf{p}_0 = (1, 1, 0)$ (blue), respectively representing spins pointing to the direction of angles $\pi/3$, $\pi/6$, and 0 to z axis. Thus, they will give a typical description of the effect of different initial states. We see that the phase boundaries are strongly modified at nonzero ω for different initial states. This may be attributed to the fact that our criteria to determine the boundary between polarized phase and unpolarized phase is too sensitive to the initial state. In contrast, the boundary between the unpolarized phase and antipolarized phase is a little bit more robust, as shown by the red line. Nevertheless, deep inside the three phases, the probability distributions of ferromagnetic order and antiferromagnetic order are still very well distinguished, indicating that the description of single-qubit dynamics in terms of the language of phase transition is still very useful.

Second, we discuss the case with nonzero relaxation rate. In general, relaxation is induced by the interaction of the qubit system with the environment and is described by the Lindblad master equation [15]. It can include very different kinds of mechanisms and channels by introducing different jump operators. The quantum measurement effect we have discussed in the paper can also be integrated into the Lindblad equation. Besides that, we want to further consider the other channels like phase damping effect induced by the environment. In the limit of thermal bath with high temperature and in the limit of weak interaction, the relaxation rate r can be introduced phenomenologically in the quantum master equation:

$$\frac{d}{dt}\hat{\rho} = -\frac{i}{\hbar}[\hat{H}, \hat{\rho}] - r(\hat{\rho} - \hat{\rho}^{(th)}) \quad (37)$$

with $\hat{\rho}^{(th)} = \hat{1}/2$ being the density matrix for the totally thermalized state. Repeating the same procedure as in Sec. II, we obtain that the evolving equation for state vector \mathbf{p}_n should be modified as

$$\mathcal{A}_\alpha = \frac{1}{2} \begin{pmatrix} 1 & \alpha \sin \theta \cos \omega e^{-r\tau} & -\alpha \sin \theta \sin \omega e^{-r\tau} \\ \alpha \sin \theta & \cos \omega e^{-r\tau} & -\sin \omega e^{-r\tau} \\ 0 & \cos \theta \sin \omega e^{-r\tau} & \cos \theta \cos \omega e^{-r\tau} \end{pmatrix}. \quad (38)$$

Using the same recursion relations and Eq. (38), we plot the phase diagram for the case of nonzero relaxation rate in Fig. 4(b). We see that when the relaxation rate is increased, the oscillation behavior in the phase diagram becomes more amplified. To qualitatively understand this intriguing behavior, one can resort to Eq. (24) which describes the effective long-range and oscillating coupling between on-site spins and can thus give rise to the oscillating behavior of phase boundary, as explained in Sec. IV C. With the presence of relaxation, one can imagine from Eq. (38) that relaxation rate r serves as an effective, but imaginary, Larmor precessing frequency, as can be seen that r always appear together with ω in \mathcal{A}_α . When the imaginary part of ω comes into the cosine function in Hamiltonian (24), it turns to a hyperbolic cosine (cosh) function, and the coupling strength is still oscillating as a function of lattice distance but its amplitude is now much more magnified. Therefore, the oscillation of phase boundary is amplified. However, as long as the relaxation rate is sufficiently small, it does not change the phase boundary.

VI. CONCLUSION

In conclusion, in this paper, we have studied the phase transitions induced by quantum measurement on a single qubit that is precessing around an external magnetic field. The corresponding phase diagram is obtained numerically by a fast algorithm we developed. By resorting to a long-range interacting Ising model, and the full counting statistical approach, the phase diagram can be quantitatively understood. The presence of magnetic field serves as an additional degree of freedom and can be easily achieved and controlled in the experiment. Our findings deepen the understanding of phase

transition induced by quantum measurement and may shed light on the characterization and monitoring of quantum state evolution [49,50] and find its future application in quantum tomography and quantum sensing.

ACKNOWLEDGMENTS

F.L. was supported by NSFC (No. 11905054) and by the Fundamental Research Funds for the Central Universities from China.

-
- [1] M. Schlosshauer, Decoherence, the measurement problem, and interpretations of quantum mechanics, *Rev. Mod. Phys.* **76**, 1267 (2005).
- [2] W. H. Zurek, Decoherence, einselection, and the quantum origins of the classical, *Rev. Mod. Phys.* **75**, 715 (2003).
- [3] M. D. Srinivas, *Measurements and Quantum Probabilities* (Universities Press, Hyderabad, India, 2001).
- [4] M. R. Pahlavani, *Measurements in Quantum Mechanics* (In-Tech, Rijeka, Croatia, 2012).
- [5] M. A. Nielsen and I. L. Chuang, *Quantum Computation and Quantum Information* (Cambridge University Press, Cambridge, UK, 2000).
- [6] N. Gisin, G. Ribordy, W. Tittel, and H. Zbinden, Quantum cryptography, *Rev. Mod. Phys.* **74**, 145 (2002).
- [7] C. L. Degen, F. Reinhard, and P. Cappellaro, Quantum sensing, *Rev. Mod. Phys.* **89**, 035002 (2017).
- [8] J. M. Elzerman, R. Hanson, L. H. W. van Beveren, B. Witkamp, L. M. K. Vandersypen, and L. P. Kouwenhoven, Single-shot read-out of an individual electron spin in a quantum dot, *Nature (London)* **430**, 431 (2004).
- [9] A. N. Vamivakas, C.-Y. Lu, C. Matthiesen, Y. Zhao, S. Fält, A. Badolato, and M. Atatüre, Observation of spin-dependent quantum jumps via quantum dot resonance fluorescence, *Nature (London)* **467**, 297 (2010).
- [10] P. Neumann, J. Beck, M. Steiner, F. Rempp, H. Fedder, P. R. Hemmer, J. Wrachtrup, and F. Jelezko, Single-shot readout of a single nuclear spin, *Science* **329**, 542 (2010).
- [11] A. Morello, J. J. Pla, F. A. Zwanenburg, K. W. Chan, K. Y. Tan, H. Huebl, M. Möttönen, C. D. Nugroho, C. Yang, J. A. van Donkelaar, A. D. C. Alves, D. N. Jamieson, C. C. Escott, L. C. L. Hollenberg, R. G. Clark, and A. S. Dzurak, Single-shot readout of an electron spin in silicon, *Nature (London)* **467**, 687 (2010).
- [12] L. Jiang, J. S. Hodges, J. R. Maze, P. Maurer, J. M. Taylor, D. G. Cory, P. R. Hemmer, R. L. Walsworth, A. Yacoby, A. S. Zibrov, and M. D. Lukin, Repetitive readout of a single electronic spin via quantum logic with nuclear spin ancillae, *Science* **326**, 267 (2009).
- [13] A. Bechtold, D. Rauch, F. Li, T. Simmet, P. Ardelt, A. Regler, K. Mueller, Nikolai A. Sinitsyn, and J. J. Finley, Three stage decoherence dynamics of electron spin qubits in an optically active quantum dot, *Nat. Phys.* **11**, 1005 (2015).
- [14] A. Bechtold, F. Li, Kai Muller, T. Simmet, P.-L. Ardelt, J. J. Finley, and N. A. Sinitsyn, Quantum Fingerprints in Higher Order Correlators of a Spin Qubit, *Phys. Rev. Lett.* **117**, 027402 (2016).
- [15] H. M. Wiseman and G. J. Milburn, *Quantum Measurement and Control* (Cambridge University Press, Cambridge, UK, 2010).
- [16] P. Goetsch and R. Graham, Linear stochastic wave equations for continuously measured quantum systems, *Phys. Rev. A* **50**, 5242 (1994).
- [17] S. A. Gurvitz, Measurements with a noninvasive detector and dephasing mechanism, *Phys. Rev. B* **56**, 15215 (1997).
- [18] A. N. Korotkov, Continuous quantum measurement of a double dot, *Phys. Rev. B* **60**, 5737 (1999).
- [19] R.-B. Liu, S.-H. Fung, H.-K. Fung, A. N. Korotkov, and L. J. Sham, Dynamics revealed by correlations of time-distributed weak measurements of a single spin, *New J. Phys.* **12**, 013018 (2010).
- [20] A. N. Korotkov, Selective quantum evolution of a qubit state due to continuous measurement, *Phys. Rev. B* **63**, 115403 (2001).
- [21] A. N. Korotkov and A. N. Jordan, Undoing a Weak Quantum Measurement of a Solid-State Qubit, *Phys. Rev. Lett.* **97**, 166805 (2006).
- [22] M. S. Blok, C. Bonato, M. L. Markham, D. J. Twitchen, V. V. Dobrovitski, and R. Hanson, Manipulating a qubit through the backaction of sequential partial measurements and real-time feedback, *Nat. Phys.* **10**, 189 (2014).
- [23] A. C. J. Wade, J. F. Sherson, and K. Molmer, Squeezing and Entanglement of Density Oscillations in a Bose-Einstein Condensate, *Phys. Rev. Lett.* **115**, 060401 (2015).
- [24] Y. Ashida and M. Ueda, Multiparticle quantum dynamics under real-time observation, *Phys. Rev. A* **95**, 022124 (2017).
- [25] Y. Ashida and M. Ueda, Full-Counting Many-Particle Dynamics: Nonlocal and Chiral Propagation of Correlations, *Phys. Rev. Lett.* **120**, 185301 (2018).
- [26] A. N. Jordan and M. Buttiker, Quantum nondemolition measurement of a kicked qubit, *Phys. Rev. B* **71**, 125333 (2005).
- [27] A. A. Clerk, M. H. Devoret, S. M. Girvin, F. Marquardt, and R. J. Schoelkopf, Introduction to quantum noise, measurement, and amplification, *Rev. Mod. Phys.* **82**, 1155 (2010).
- [28] P. C. Maurer, G. Kucsko, C. Latta, L. Jiang, N. Y. Yao, S. D. Bennett, F. Pastawski, D. Hunger, N. Chisholm, M. Markham, D. J. Twitchen, J. I. Cirac, and M. D. Lukin, Room-temperature quantum bit memory exceeding one second, *Science* **336**, 1283 (2012).
- [29] G.-Q. Liu, J. Xing, W.-L. Ma, P. Wang, C.-H. Li, H. C. Po, R.-B. Liu, and X.-Y. Pan, Single-Shot Readout of a Nuclear Spin Weakly Coupled to a Nitrogen-Vacancy Center, *Phys. Rev. Lett.* **118**, 150504 (2017).
- [30] T. Gefen, M. Khodas, L. P. McGuinness, F. Jelezko, and A. Retzker, Quantum spectroscopy of single spins assisted by a classical clock, *Phys. Rev. A* **98**, 013844 (2018).
- [31] A. L. Balk, Fuxiang Li, I. Gilbert, J. Unguris, N. A. Sinitsyn, and S. A. Crooker, Broadband Spectroscopy of Thermodynamic Magnetization Fluctuations Through a Ferromagnetic Spin-Reorientation Transition, *Phys. Rev. X* **8**, 031078 (2018).
- [32] K. S. Cujia, J. M. Boss, K. Herb, J. Zopes, and C. L. Degen, Tracking the precession of single nuclear spins by weak measurements, *Nature* **571**, 230 (2019).

- [33] F. Li, S. A. Crooker, and N. A. Sinitsyn, Higher order spin noise spectroscopy of atomic spins in fluctuating external fields, *Phys. Rev. A* **93**, 033814 (2016).
- [34] P. Wang, C. Chen, X. Peng, J. Wrachtrup, and R.-B. Liu, Characterization of Arbitrary-Order Correlations in Quantum Baths by Weak Measurement, *Phys. Rev. Lett.* **123**, 050603 (2019).
- [35] F. Sakuldee and L. Cywiński, Characterization of a quasi-static environment with a qubit, *Phys. Rev. A* **99**, 062113 (2019).
- [36] J. P. Garrahan and I. Lesanovsky, Thermodynamics of Quantum Jump Trajectories, *Phys. Rev. Lett.* **104**, 160601 (2010).
- [37] G. Mazzucchi, W. Kozłowski, S. F. Caballero-Benitez, T. J. Elliott, and I. B. Mekhov, Quantum measurement-induced dynamics of many-body ultracold bosonic and fermionic systems in optical lattices, *Phys. Rev. A* **93**, 023632 (2016).
- [38] Y. Li, X. Chen, and M. P. A. Fisher, Quantum Zeno effect and the many-body entanglement transition, *Phys. Rev. B* **98**, 205136 (2018).
- [39] Y. Ashida, S. Furukawa, and M. Ueda, Parity-time-symmetric quantum critical phenomena, *Nat. Commun.* **8**, 15791 (2017).
- [40] O. Oreshkov and T. A. Brun, Weak Measurements are Universal, *Phys. Rev. Lett.* **95**, 110409 (2005).
- [41] A. N. Jordan and A. N. Korotkov, Qubit feedback and control with kicked quantum nondemolition measurements: A quantum Bayesian analysis, *Phys. Rev. B* **74**, 085307 (2006).
- [42] A. Chantasri, J. Dressel, and A. N. Jordan, Action principle for continuous quantum measurement, *Phys. Rev. A* **88**, 042110 (2013).
- [43] A. Chantasri and A. N. Jordan, Stochastic path-integral formalism for continuous quantum measurement, *Phys. Rev. A* **92**, 032125 (2015).
- [44] W.-L. Ma, P. Wang, W.-H. Leong, and R.-B. Liu, Phase transitions in sequential weak measurements, *Phys. Rev. A* **98**, 012117 (2018).
- [45] C. Presilla, R. Onofrio, and U. Tambini, Measurement quantum mechanics and experiments on quantum Zeno effect, *Ann. Phys.* **248**, 95 (1996).
- [46] F. Li, J. Ren, and N. A. Sinitsyn, Quantum Zeno effect as a topological phase transition in full counting statistics and spin noise spectroscopy, *Europhys. Lett.* **105**, 27001 (2014).
- [47] L. D. Landau and E. M. Lifshitz, *Quantum Mechanics: Non-relativistic Theory*, 3rd ed. (Butterworth-Heinemann, New York, 1981), Vol. 3.
- [48] Y. V. Nazarov, *Quantum Noise in Mesoscopic Physics* (Kluwer, Dordrecht, 2003).
- [49] M. Pfender, P. Wang, H. Sumiya, S. Onoda, W. Yang, D. B. R. Dasari, P. Neumann, X.-Y. Pan, J. Isoya, R.-B. Liu and J. Wrachtrup, High-resolution spectroscopy of single nuclear spins via sequential weak measurements, *Nat. Commun.* **10**, 594 (2019).
- [50] F. Li, V. Y. Chernyak, and N. A. Sinitsyn, Quantum Annealing and Thermalization: Insights from Integrability, *Phys. Rev. Lett.* **121**, 190601 (2018).